8th International Colloquium on Bluff Body Aerodynamics and Applications
Northeastern University, Boston, Massachusetts, USA
June 7 - 11, 2016

Comparative Study of Semi-analytical and Numerical Methods for Aerodynamic Analysis of Long-span Bridges

I. Kavrakov[a,*], K. Ibrahim[b], G. Morgenthal[c]

[a]*Research Training Group 1462, Bauhaus University, Weimar, Germany,*
igor.kavrakov@uni-weimar.de
[b]*Chair of Modelling and Simulation of Structures, Bauhaus Universiy, Weimar, Germany,*
khaled.ibrahim.tolba@uni-weimar.de
[c]*Chair of Modelling and Simulation of Structures, Bauhaus University, Weimar, Germany,*
guido.morgenthal@uni-weimar.de

SUMMARY:
Wind-induced vibrations commonly are the leading design criterion for long-span bridges. This article presents a comparative study between a recently developed quasi-3D turbulent Computational Fluid Dynamics (CFD) scheme based on the Vortex Particle Method (VPM) and various semi-analytical models based on a flat-plate aerodynamics. The models are compared under turbulent wind for various wind speeds for a 2D case including a flutter analysis. A quasi-3D turbulent analysis is also conducted. The aerodynamic coefficients are identified from a CFD analysis and compared against experimental results along with qualitative and quantitative assessment of the turbulence field.The Great Belt East Bridge was chosen as a reference object.

Keywords: Buffeting, Aerodynamic modeling, CFD, VPM, Long-span Bridges

1. INTRODUCTION

The leading load-case scenario for the design of long-span bridges are the wind-induced vibrations. High Reynolds number, irregular shape with regions of massive flow separation and large time-scales are only few of the many reasons why the modeling of the Fluid-Structure Interaction (FSI) for this type of bluff bodies has been an ongoing research topic in the last few decades. Generally, the FSI is simulated using three models: experimental, numerical and semi-analytical. The experimental aeroelastic testing still represents the benchmark for design; however, the time consuming and expensive procedure is a disadvantage. The semi-analytical approach of modeling of the aerodynamic forces offers fast and robust prediction of the response. In this case, experimental aerodynamic coefficients are necessary for the semi-analytical models to describe the complex aerodynamic behaviour. With the ascent of the computer technology, the numerical models based on CFD have attracted considerable attention. Here, the Navier-Stokes (N-S) equations describing the fluid domain are discretized resulting in an independent numerical procedure from wind tunnel tests. Nevertheless, the numerical uncertainty is a primary set-back and thus, there is a great deal of scepticism towards their practical implementation.

This paper presents a comparison of the response of a suspension bridge subjected to turbulent wind between semi-analytical models and a recently developed quasi-3D turbulent scheme based on the VPM. The goal is to qualitatively and quantitatively verify the CFD scheme for buffeting analysis by the semi-analytical models from an aspect of their implied assumptions. The aerodynamic coefficients and the flutter limit are identified by CFD and verified with wind tunnel results.

2. AERODYNAMIC MODELS

2.1. Semi-Analytical Models

The semi-analytical models are commonly based on analytical expressions from flat-plate aerodynamics and aerodynamic coefficients to account for the bluffness of the bridge deck. The quasi-steady and linear unsteady assumptions are the two main pivotal points around which the semi-analytical models are developed. The first assumption neglects the fluid memory, while the latter ignores the aerodynamic nonlinearity. The following aerodynamic models were used within this study: the Quasi-Steady (QS), the Linearized Quasi-Steady (LQS), the Corrected Quasi-Steady (CQS) (Diana et al., 1993), the Linearized Unsteady (LU) (Chen and Kareem, 2002) with its simplification for the Mode By Mode (MBM) approach, the Modified Quasi-Steady (MQS)(Øiseth et al., 2010) and the Hybrid Nonlinear (HNL) model (Wu and Kareem, 2013). Fig. 1 depicts the forces acting on a bridge deck under the the mean wind speed U with a horizontal $u(t)$ and a vertical $w(t)$ turbulent component (buffeting forces) including motion-induced forces due to lateral p, vertical h and torsional motion α. This includes the drag F_D, lift F_L and the moment F_M forces.

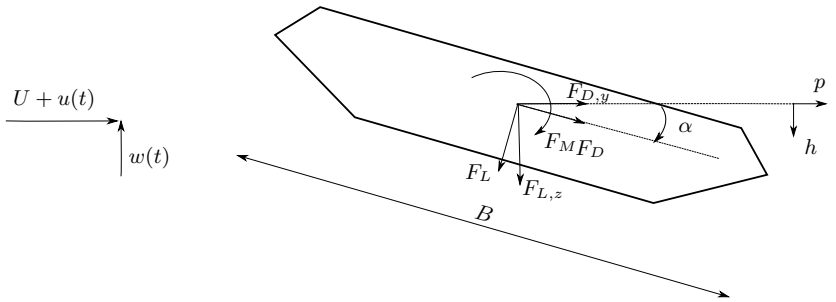

Figure 1. Aerodynamic forces acting on a bridge deck.

The QS model takes into account the aerodynamic nonlinearity; however it fails to describe the fluid-memory effect. It does not present an implementation overhead and the uncertainty that arises with its input parameters is low, except the m_i, $i \in \{h, \alpha\}$ coefficient defining the aerodynamic centrer. The lift force F_L, resultant velocity V_{res} and effective angle of attack $\alpha_{e,i}$ are described as:

$$F_L = -\frac{1}{2}\rho V_r^2 B C_L(\alpha_e),\ V_{res} = \sqrt{(U+u-\dot{p})^2 + (w+\dot{h}+m_i B\dot{\alpha})},\ \alpha_{e,i} = \alpha_s + \alpha + \arctan\left(\frac{w+\dot{h}+m_i B\dot{\alpha}}{U+u-\dot{p}}\right), \tag{1a,1b,1c}$$

where, ρ is the air density, $C_L(\alpha_e)$ is the lift nonlinear coefficient, α_s is the angle of rotation due to mean wind forces and B is the chord. In case of the LQS model, the above equation is linearized with respect to the α_s yielding in linear relation between the lift slope $C_L^{'}|_{\alpha_s}$ and α_e. The CQS model integrates the $C_L(\alpha_e)$ over the effective angle by introducing a correction coefficient K_L^* multiplying the lift slope $C_L^{'}(\alpha_e)$. With this, the fluid memory is taken into account up to a certain degree. The lift force for the LU model is a linear function of the fluctuating wind components and the displacements with its time derivatives, which are modified by frequency dependent coefficients:

$$\begin{aligned} F_{L,z} = &-\frac{1}{2}\rho U^2 B\left(C_L + (C_L^{'} + C_D)\frac{w}{U}\chi_{Lw}(K) + C_L\frac{2u}{U}\chi_{Lu}(K)\right) \\ &+\frac{1}{2}\rho U^2 B\left(KH_1(K)\frac{\dot{h}}{U} + KH_2(K)B\frac{\dot{\alpha}}{U} + K^2H_3(K)B\alpha + K^2H_4(K)\frac{h}{U} + KH_5(K)\frac{\dot{p}}{U} + K^2H_6(K)\frac{p}{U}\right). \end{aligned} \tag{2}$$

The flutter derivatives H_i are dependent on the reduced frequency of oscillation $K = \omega B/U$ and account for the fluid memory, while the rise-time of the buffeting forces is addressed by the aerodynamic admittance functions χ. The preceding equation includes terms from the frequency and the time domain; thus, a rational approximation is required for a pure time-domain solution. In this case the impulse functions I_i were utilized, which are identified from the unsteady information contained in the flutter derivatives and the aerodynamic admittance (Chen and Kareem, 2002):

$$\begin{aligned} F_{L,z} = &-\frac{1}{2}\rho U^2 \int_{-\infty}^{t} \left(I_{L_{bu}}(t-\tau)\frac{u(\tau)}{U} + I_{L_{bw}}(t-\tau)\frac{w(\tau)}{U} \right) \mathrm{d}\tau \\ &+ \frac{1}{2}\rho U^2 \int_{-\infty}^{t} \left(I_{L_{sh}}(t-\tau)h(\tau) + I_{L_{s\alpha}}(t-\tau)\alpha(\tau) + I_{L_{sp}}(t-\tau)p(\tau) \right) \mathrm{d}\tau. \end{aligned} \tag{3}$$

The rational approximation can be a cumbersome in some cases for very bluff bodies and scattered aerodynamic derivatives. In order to alleviate this, the MQS interpolates the flutter derivatives at a chosen frequency, resulting in same formulation as LU without the lag terms in the rational approximation. For the simple MBM approach, the aerodynamic coupling is completely neglected. The most advanced model within this study is the NHL model which splits the response and wind spectrum on low and high frequency components. The QS model is utilized for the lower part since the aerodynamic nonlinearity is governing, while the LU model for the high frequencies as the fluid memory plays significant role. Recently nonlinear aerodynamic models have been developed based on Reduced Order Modeling (ROM) and approximation of the hysteresis of the dynamic wind coefficients (Wu and Kareem, 2013); however, these are beyond the scope of this study.

2.2. Vortex-Particle Method

For the solution of the N-S equations, a multitude of numerical methods exist. The choice of the suitable method is crucial for an accurate modeling of the underlying physics, while efficiently using the computational resources. The VPM uses a grid free formulation for simulating incompressible fluid flow. This mesh-less numerical technique provides an alternative to classical mesh based Eulerian methods. The VPM models vorticial flows by solving the vorticity transport equation in Lagrangian flow. These are typical flows around bluff bodies i.e. moderate to high Reynolds number. The formulation and the discretization reflect the natural representation in dominantly vortcial flow, which is inherent in flows around bluff bodies. Vortex sheets are modeled as particles with invariant strength which are transported downstream by convection and diffusion due to the induced velocity field. For inviscid flow and $\mathcal{R}^2$ from the Euler equations described by the vorticity ω eq. (4a) the velocities $\boldsymbol{u}(\boldsymbol{x_p})$ of arbitrary "fluid markers" described by their position $\boldsymbol{x_p}$ can be obtained by using the Biot-Savart equation (4b) (Morgenthal and Walther, 2007). In a domain discretized by particles, $\boldsymbol{u}(\boldsymbol{x_p})$ yields into superposition of the contributions from all of the particles depending on their position and strength Γ_p:

$$\frac{D\omega}{Dt} = 0, \quad \boldsymbol{u}(\boldsymbol{x_p}) = \boldsymbol{U} - \frac{1}{2\pi}\int_{\mathcal{D}} \frac{\boldsymbol{\omega}_0(\boldsymbol{x}_0)\times(\boldsymbol{x}_0-\boldsymbol{x})}{|\boldsymbol{x}_0-\boldsymbol{x_p}|^2}\,\mathrm{d}\mathcal{D}_0, \quad \boldsymbol{u}(\boldsymbol{x_p}) = \boldsymbol{U} - \sum_{p=1}^{N_p} K_\sigma(\boldsymbol{x}_p-\boldsymbol{x})\Gamma_p. \tag{4a,4b,4c}$$

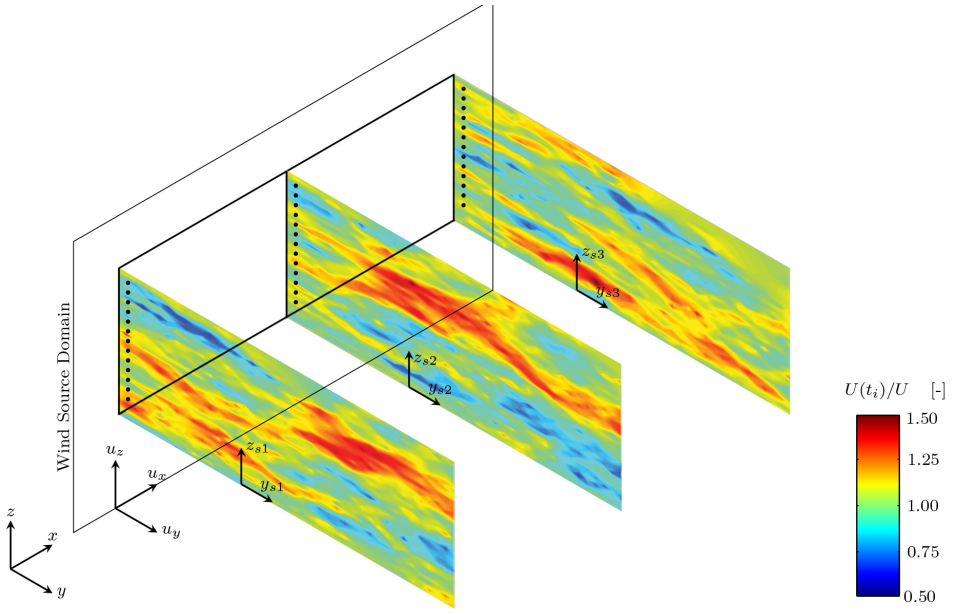

Figure 2. A snapshot of normalized instantaneous velocity field in parallel 2D slices including a schematic for particles' inflow position.

Singularities arise when two particles approach each other and thus a mollified velocity kernel is required K_σ to avoid numerical instabilities. The boundary element method was used for the FSI, discretizing the surface into panels, at which the surface pressure is computed integrating the pressure gradient. The diffusion was solved separately as a fractional step using the Random Walk Method. The method also accounts for free-space boundary conditions, leading to a robust scheme for flows around structures such as towers and bridges (Morgenthal, Corriols, et al., 2014).

One of the key point of this study is the modeling and simulation of atmospheric turbulence in VPM. Although turbulence is three dimensional by its nature, the idea is to obtain valid turbulence characteristics in a 2D slice neglecting the tilting and stretching of vortices. In some previous studies (Rasmussen et al., 2010) the velocities were sampled on a 2D ladder, from which the particles' strength was computed and the particles were injected into the domain. Although time correlation was preserved, the span-wise correlation between slices for a multi-slice simulation (Fig. 2) could not be accounted for. Therefore, in a recently developed method by the authors this was achieved by simulating and injecting particles directly instead of velocities in the domain. In order to obtain the inflow condition, a relation is required between the standard deviation of the velocity σ_U and particle's strength σ_Γ. Relating σ_U and Γ_P^i for a single point:

$$\sigma_U = \sqrt{\frac{1}{N_T}\sum_{i=1}^{N_T}\left[\sum_{p=1}^{N_p} K_\sigma(r_p)\Gamma_p^i\right]^2} \quad . \qquad \sum_{p=1}^{N_p} K_\sigma(r_p)\Gamma_p = K_\sigma(r_1)\sum_{p=1}^{N_1}\Gamma_p \cdots + K_\sigma(r_j)\sum_{p=N_{j-1}+1}^{N_p}\Gamma_p, \tag{5a,5b}$$

represents the expansion of the summation of the particles' influences on the velocity for a stabilized domain with homogeneously spaced particles at distance $r_j = j\Delta r$ where Taylor's hypothesis applies and N_j is the corresponding number of particles at the before mentioned distance. For large amount of particles N_l uncorrelated in-plane, the $\sum_{p=1}^{N_l}\Gamma_p$ could be linearly related to the summation of the total number of particles influencing the point of interest N_p (eq. (6a)). For equidistantly

spaced particles, eq. (6b) could be obtained which then can be related to eq. (5b) as:

$$\sum_{p=1}^{N_l}\Gamma_p \approx \frac{N_j}{N_p}\sum_{p=1}^{N_p}\Gamma_p, \quad \frac{N_j}{N_p}=\frac{2\pi j\Delta r}{\sum_{j=1}^{n}2\pi j\Delta r}, \quad \sum_{p=1}^{N_p}K_\sigma(r_p)\Gamma_p=\sum_{j=1}^{n}\left[K_\sigma(j\Delta r)\cdot j\right]\cdot\frac{1}{\sum_{j=1}^{n}j}\sum_{p=1}^{N_p}\Gamma_p. \tag{6a,6b,6c}$$

The first summation in the right hand side of eq. (6c) converges to $n/(2\pi\Delta r)$ for a Gaussian core. Employing eq. (6c) into eq. (5a) and expanding the finite summation over the squared term and neglecting the higher order term as cross-correlation eq. (7a) the standard deviation of the velocity fluctuation σ_u can be related to σ_Γ as (eq. (7b)):

$$\sum_{i=1}^{N_T}\left[\sum_{p=1}^{N_p}\Gamma_p^i\right]^2=\sum_{i=1}^{N_T}\sum_{p=1}^{N_p}\left(\Gamma_p^i\right)^2, \quad \sigma_U=\frac{n}{2\pi\Delta r}\cdot\left[\frac{1}{\sum_{i=1}^{n}i}\right]\cdot\sqrt{N_p}\cdot\sigma_\Gamma, \quad \sigma_\Gamma=\pi\Delta r\left[I_u U\right]. \tag{7a,7b,7c}$$

After some basic manipulations, the σ_Γ can be related to the turbulence intensity I_u (eq. (7c)).
As a result, the standard deviation of the particles' strength could be simulated as a random correlated process and thus correlated particles along the bridge axis for each slice could be obtained. An obvious shortcoming to this method is that once the particles are into the domain, there is no interaction between them from different slices. Furthermore for FSI of a line-like structure, the correlation of the buffeting forces can not be taken into account as they can not be separated from the self-excited forces in the fully coupled CFD. However, the concept of the joint acceptance for high wind speed and coupled effects is a further topic of research.

3. APPLICATION

3.1. Reference Object

The Great-Belt East bridge is used as a reference object (Fig. 3) with a 31 m wide cross section (Fig. 1). In the analysis, 22 mode-shapes were included with frequencies ranging from 0.05Hz up to 0.5Hz. The frequencies and wind tunnel data were validated against (Larsen, 1992). Modal damping of 0.5% modal damping was used with m = 22.7 t/m and I_α = 2240 tm^2.

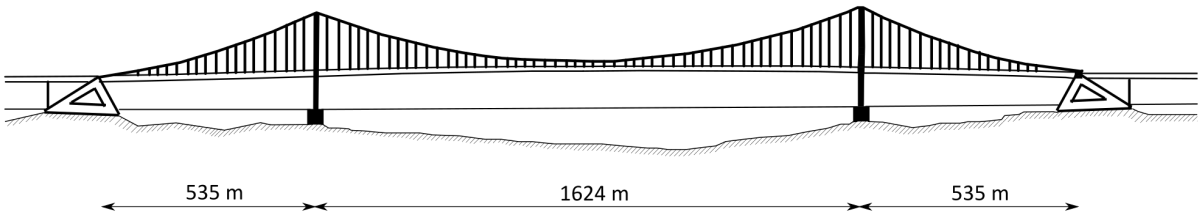

Figure 3. Reference object - Great Belt East Bridge.

3.2. 2D Sectional Analysis

3.2.1. Static wind coefficients and flutter derivatives

On Figure 4 (left) the domain of the CFD simulations is depicted. The simulations were conducted for Re=10^5 for the static wind coefficients and flutter derivatives and up to Re=10^8 for the buffeting analysis. The static wind coefficients and flutter derivatives were obtained for laminar flow. The C_L

and C_M are almost in perfect alignment with the experiments, as shown on Figure 4 (right). Some discrepancies are noted in the C_D. Possible reasons for the discrepancies could be the modeling of railings and inflow turbulence in the experiments. In this study C_D could be further improved, as the friction drag was neglected during the determination procedure. The flutter derivatives seem to be in good agreement with the experiments, as shown on Figure 5. The flutter derivatives were obtained also for different angle of attack (Fig. 9).

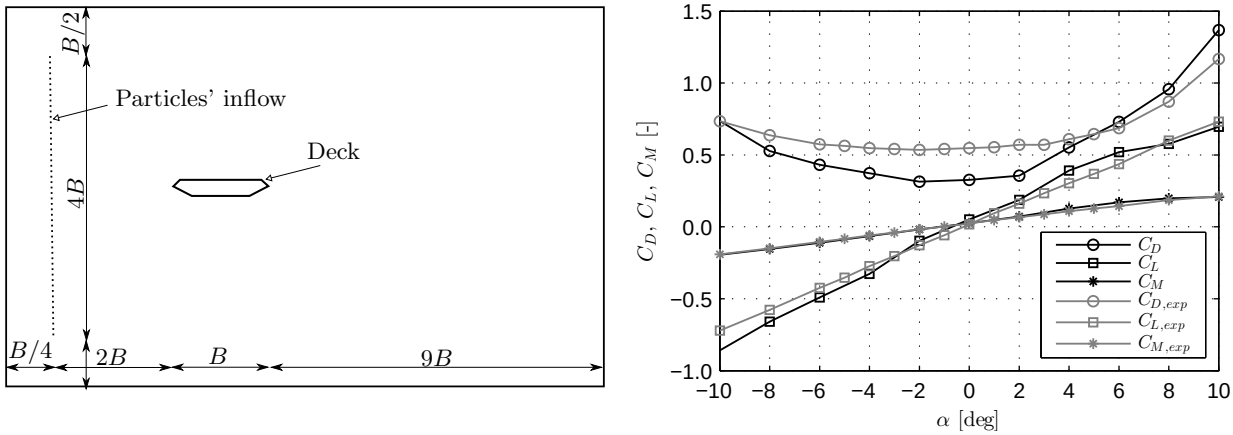

Figure 4. Simulation domain (left) and comparison of static wind coefficients with experimental data (right).

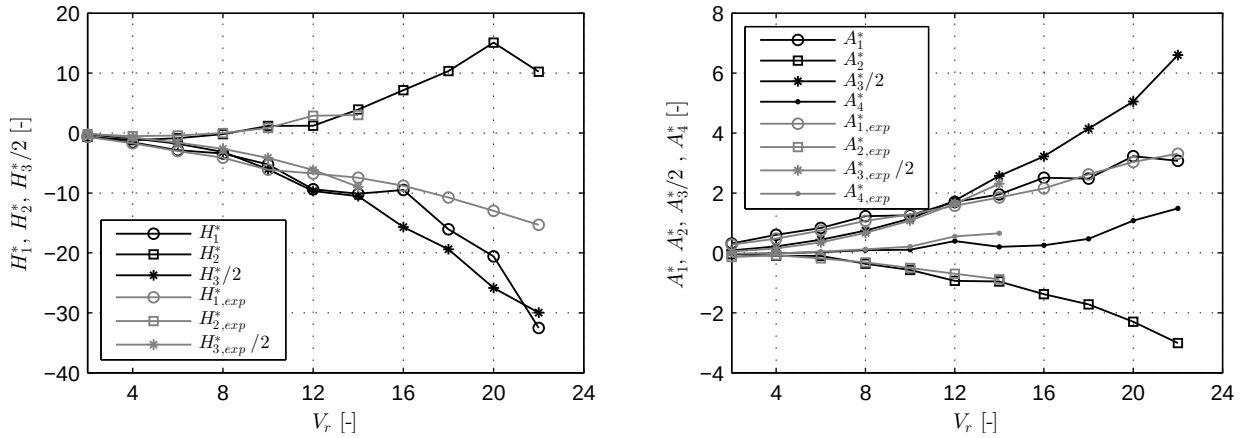

Figure 5. Comparison of the flutter derivatives with experimental data for α=0 deg.

3.2.2. Flow field validation

In case of turbulent flow, the distance between the particle injection and tip of the cross section should be longer than laminar flow. The best way to be determined is to perform a parametric study of the properties of the turbulent field such as the Power Spectral Density (PSD) and the turbulence intensity. Similar one was conducted by Rasmussen et al., 2010. As a target spectrum, the von Karman was chosen with 6% turbulence. Figure 6 (right) depicts snapshot of a turbulent flow, where the inflow particles are visible. On Figure 6 normalized mean wind speed and is depicted w.r.t a portion of the domain, representing free stream velocity accurately. On Figure 7 the normalized turbulence intensities measured at the windward tip of the section (placed at x=0, y=0) are depicted. The measured I_u was higher for 10%, while for I_w the difference was 8%.

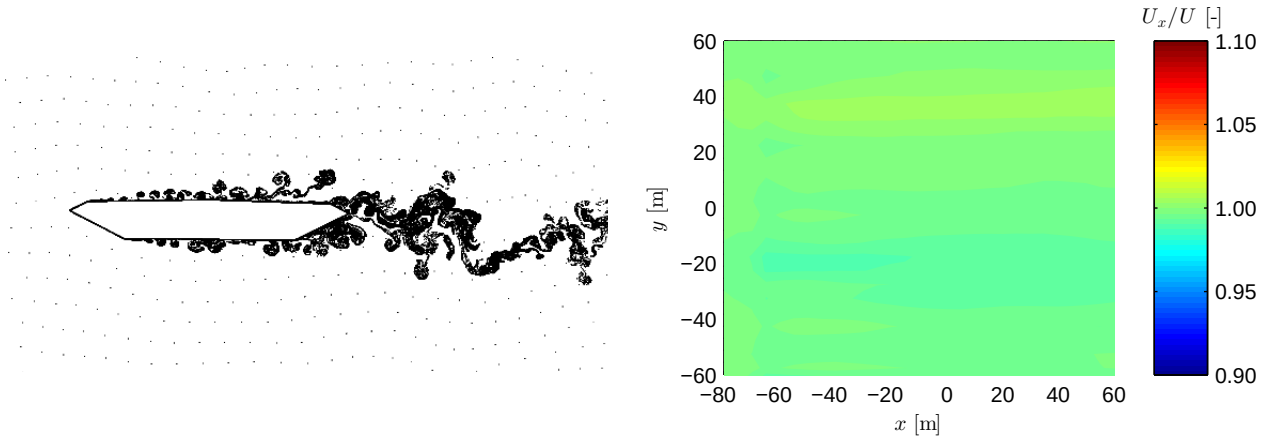

Figure 6. Snapshot of turbulent flow field (left). Normalized mean wind speed w.r.t. U=40 m/s for a portion of the domain for U_u (right).

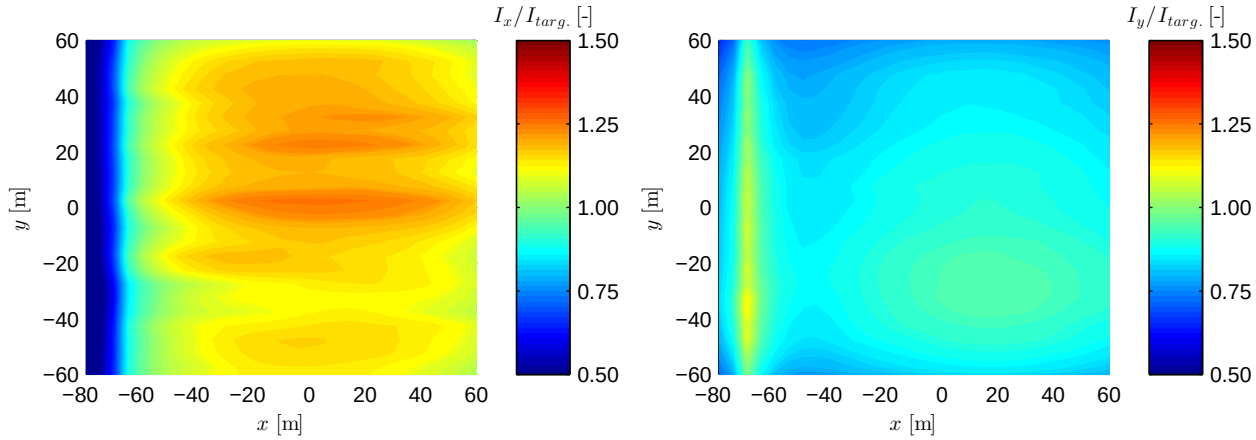

Figure 7. Normalized turbulence intensity w.r.t. I_u=6% for a portion of the domain for I_u (left) and I_w (right).

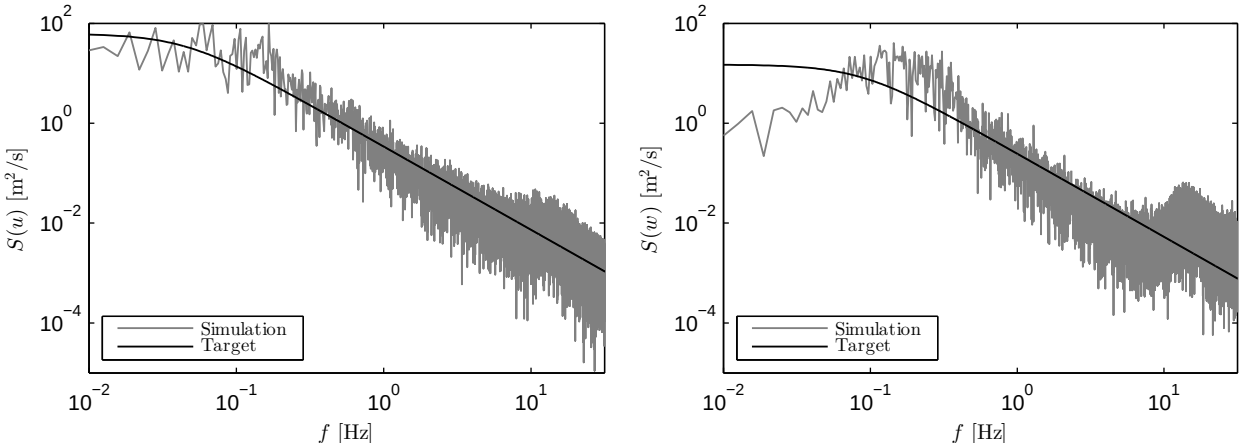

Figure 8. PSD of the longitudinal $S(u)$ (left) and vertical $S(w)$ (right) component w.r.t. von Karman for I_u=I_w=6%.

On Figure 8 the comparison between the target PSD and measured one is depicted. The longitudinal spectra (left) coincides slightly better than the vertical one (right) w.r.t. target PSD. The distinctive artificial peak and increase in the energy near 10 Hz is due to the chosen seeding frequency Δ_p=10. For now the variation of ±10% in the I and discrepancy in the PSD are acceptable; however, further parametric studies w.r.t. numerical parameters such as section position, grid dimensions and particle seeding frequency would lead to higher quality of the turbulent flow field.

3.2.3. Aerodynamic analysis

Flutter and buffeting analysis were conducted for a single slice with 1 m reference length. The flutter limit for laminar flow for CFD and various semi-analytical models are shown in Figure 9 (right). Most of the models coincide good with Wind Tunnel (WT) and CFD results, except for the MBM model for which flutter limit could not be determined, since it is a coupled flutter. The LQS and MQS flutter limits were obtained with aerodynamic centre obtained from the flutter derivatives at V_r = 20 for the heaving and pitching motion. On the same figure the critical flutter velocities are obtained for the commonly used aerodynamic centre of m_α=-0.25 which corresponded to the lower values. It should be noted that the fluid memory is crucial in many cases and LQS and QS do not predict the flutter limit accurately, and should be used with precaution (Chen and Kareem, 2002). Figure 13 depicts the Root Mean Square (RMS) of the vertical (left) and rotational (right) displacement. It should be noted that buffeting analysis, unlike other aeroelastic results, needs to be interpreted and corrected for non-similarities.These non-similarities arise influence of mode shapes, displacement and the torsional damping.

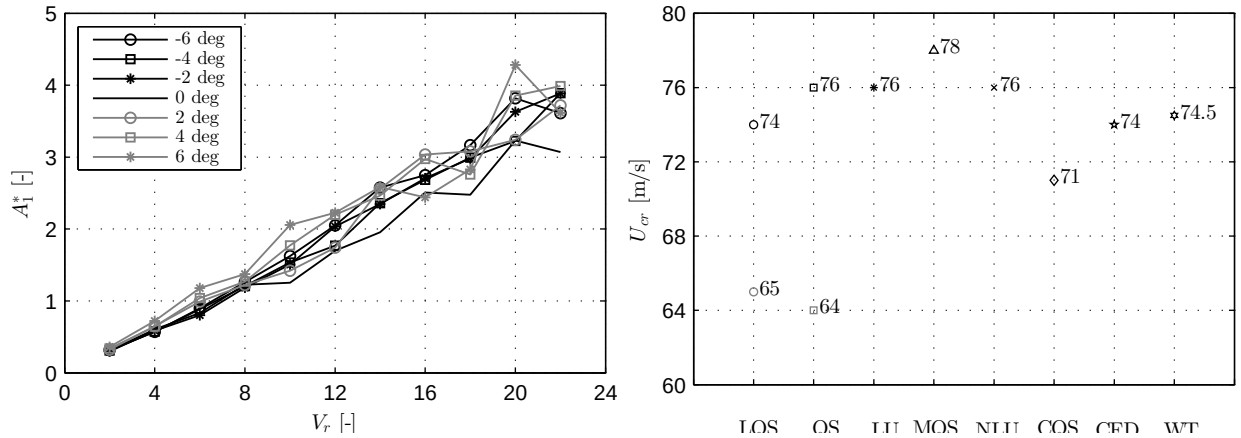

Figure 9. Flutter Derivative A_1^* for different angle of incidence (left). Critical flutter velocity for 2D analysis (right). WT stands for Wind Tunnel results. The grey markers for LQS and QS are for aerodynamic centre m = 0.25.

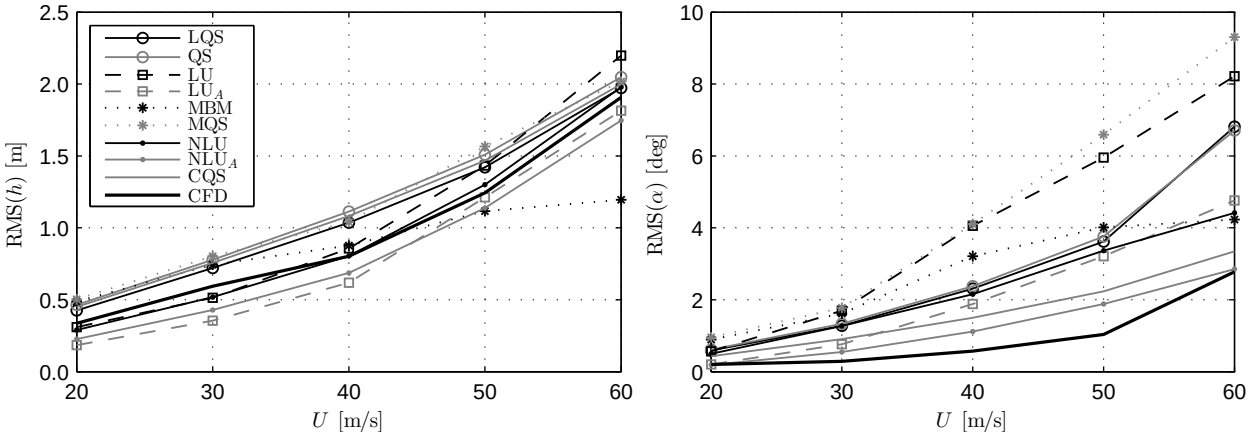

Figure 10. RMS of vertical (left) and torsional (right) displacements for various models for 2D analysis. The Subscript A accounts for the Sears' admittance.

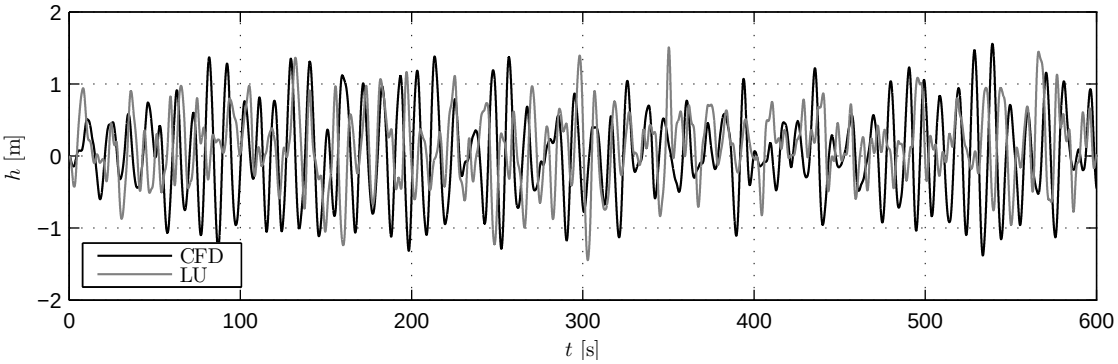

Figure 11. Comparison of the time history of the vertical displacement for CFD and LU for U = 30 m/s.

The RMS of the vertical displacements are quite comparable. The QS amplitudes are the highest with negligible difference with the CQC. The LU model experiences somewhat higher amplitudes than the NLU. The CFD analysis is somewhere in-between LU and LU$_A$, which takes into account the Sears' admittance. This is somehow realistic as the streamed-lined sections behaviour is close to a flat-plate and overshooting is not expected. In the high velocity range, the situation changes due to the influence of the aerodynamic coupling, as the rotational displacements are significantly large. Although some of the advanced models (NLU$_A$) are comparable with the CFD analysis some of the results such as the high amplitudes of the LU model needs to be further revised. However, it is possible that this is due to the high rotational displacements for which, the LU might not replicate the torsional damping due to the amplitude. Another reason for higher rotational displacements of the LU over the QS and LQS could be the overshooting. This is less likely for a streamed-lined section. Figure 11 depicts comparable time histories of the vertical displacement.

3.3. Quasi-3D Analysis

The whole point of quasi-3D CFD analysis is to be able to perform a buffeting analysis, at reasonable computational cost, without obtaining the aerodynamic coefficients. For this, here a multi-slice simulation is conducted with 9 slices applying wind only on deck. The slices locations and results for U=60 m/s are depicted on Figure 12 for the vertical (left) and torsional (right) displacements. The vertical displacements correspond well with the CFD. Due to the high reduced velocity the effect of aerodynamic admittance is negligible for the LU model for the vertical displacement.

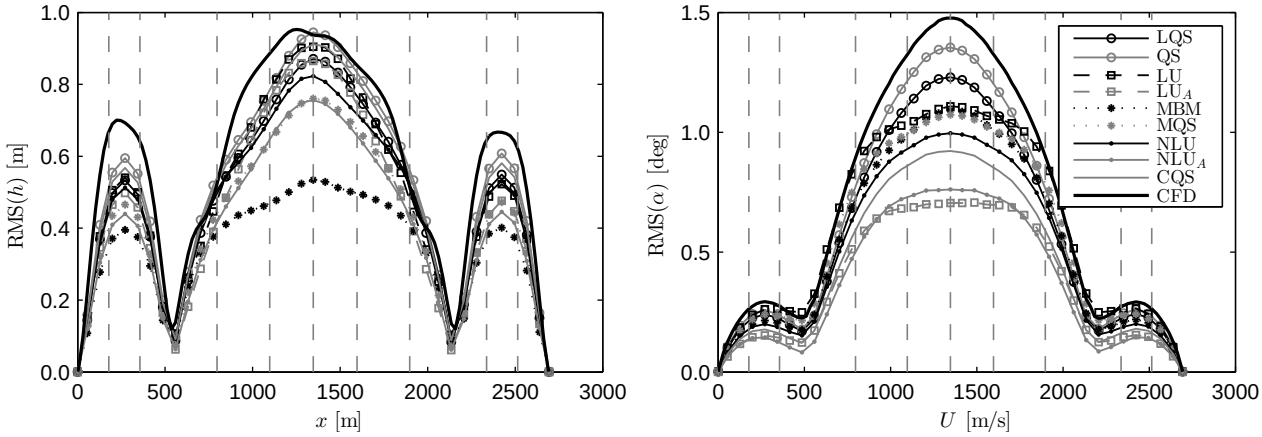

Figure 12. Root Mean Square (RMS) of vertical (left) and torsional (right) displacement for U=60 m/s. The Subscript "A" denotes the Sears' admittance. The dashed grey lines note the slices' location.

The effect of aerodynamic coupling is obvious by considering the MBM model. The reason for the discrepancies between the CFD and the rest of the models for the vertical displacement could that the slices' location and particularly the number of slices is not optimal and should be studied in depth, as well as the quality of the flow characteristics. The comparison among the semi-analytical models is quite logical, as mostly the QS and LQS exhibit higher displacements than the LU and NLU. The aerodynamic admittance decreases the torsional response significantly in this case and the reduction factor from the CQS is more evident for the rotational displacements. Similar observations are done by Wu and Kareem, 2013.

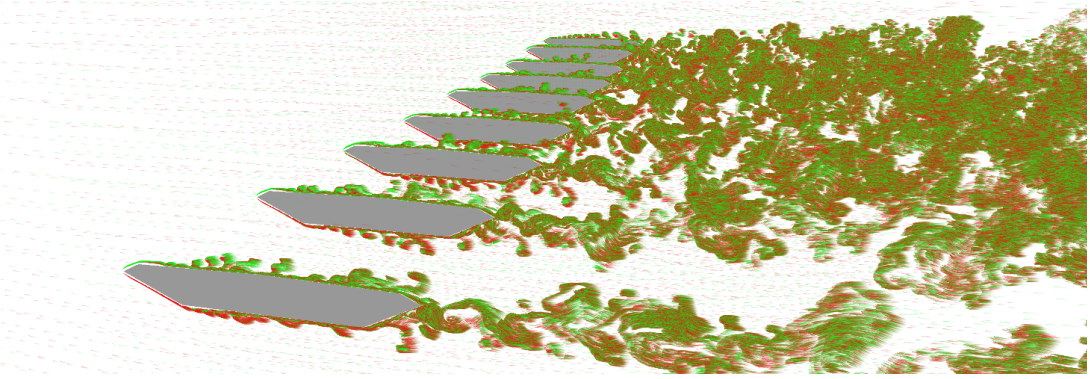

Figure 13. An instantaneous particle stream of the quasi-3D buffeting analysis.

4. CONCLUSION

In this study, a comparative analysis was conducted based on numerical and semi-analytical models for aerodynamic analysis of long-span bridges. The semi-analytical models present a robust and reliable estimate of the response; however, they are highly dependent on the aerodynamic coefficients and as the complexity of the model increases, numerical uncertainties arise. The recently developed scheme for quasi-3D buffeting analysis based on the VPM resulted in comparable results with the semi-analytical models. The advantage is that few parameters are required to describe the response over the whole wind range and its highly computational efficient. However, there is a great deal of numerical uncertainty and further validation and best-practice studies are required.

REFERENCES

Chen, X. and Kareem, A. 2002. Advances in Modeling of Aerodynamic Forces on Bridge Decks. Journal of Engineering Mechanics 128, 1193–1205.

Diana, G., Bruni, S., Cigada, A., and Collina, A. 1993. Turbulence effect on flutter velocity in long span suspended bridges. Journal of Wing Engineering and Industrial Aerodynamics 48, 329–342.

Larsen, A., ed. 1992. *Aerodynamics of Large Bridges*. Balkema, Rotterdam, Copenhagen.

Morgenthal, G., Corriols, A. S., and Bendig, B. 2014. A GPU-accelerated pseudo-3D vortex method for aerodynamic analysis. Journal of Wind Engineering and Industrial Aerodynamics 125, 69–80.

Morgenthal, G. and Walther, J. H. 2007. An immersed interface method for the Vortex-In-Cell algorithm. Computers and Structures 85, 712–726.

Øiseth, O., Rönnquist, A., and Sigbjörnsson. 2010. Simplified prediction of wind-induced response and stability limit of slender long-span suspension bridges, based on quasi-steady theory: A case study. Journal of Wind Engineering and Industrial Aerodynamics 98, 730–741.

Rasmussen, J., Hejlesen, M., Larsen, A., and Walther, J. 2010. Discrete vortex method simulations of the aerodynamic admittance in bridge aerodynamics. Journal of Wind Engineering and Industrial Aerodynamics 98, 754–766.

Wu, T. and Kareem, A. 2013. Bridge aerodynamics and aeroelasticity: A comparison of modeling schemes. Journal of Fluids and Structures 43, 347–370.